

In vivo study of human mandibular distraction osteogenesis. Part I: Bone transport force determination

ANNE-SOPHIE BONNET^{1*}, GUILLAUME DUBOIS², PAUL LIPINSKI¹, THOMAS SCHOUMAN³

¹ Laboratory of Mechanics, Biomechanics, Polymers and Structures, Ecole Nationale d'Ingénieurs de Metz, Metz, France.

² Orthopédie Biomécanique Locomotion, Chatillon, France.

³ AP-HP, Department of Maxillofacial Surgery, Pitié-Salpêtrière University Hospital, Faculty of Medicine, Paris, France.

Distraction Osteogenesis (DO) is a surgical technique used to reconstruct bone defects. The evolution of forces acting during DO is known to be strongly influencing the clinical issue of the treatment. The aim of this study was to determine experimentally the time-dependent forces imposed on bone regenerate by a distraction device in the case of a mandibular DO consecutive to a gunshot wound. To evaluate the bone transport forces, some fixing pins of the distraction device were equipped with strain gauges. Measurements were done during the first weeks of the treatment. An equilibrium analysis was achieved to determine the forces acting in bone regenerate from strains in the pins. Those quantities evolved during the records approximately from 5 N to 3–4 N and 2 N to 0–0.3 N for the tension and shear forces, respectively, depending on the record duration. For the longest record, the callus lengthening reached 0.17 mm during 75 minutes. This decrease of force and simultaneous callus extension can be attributed to the viscosity of regenerate and the elastic energy release of the device. Essential data were obtained concerning forces, extension and their evolution during mandibular DO. The low force level obtained was attributed to the absence of resistance of the soft tissues in the case of ballistic trauma restoration.

Key words: experimental method, mandibular distraction osteogenesis, transport force

1. Introduction

Distraction osteogenesis (DO) consists in the lengthening of a bone by means of a mechanical device. Bone is split into two parts and one is then moved away from the other at an adapted rate. If this rate is too high, DO will fail to create new bone in the gap and if it is too low, exaggerated resistances in lengthening can be encountered due to early consolidation (ILIZAROV [1]). Bases for DO have been set up in the fifties of the 20th century (ILIZAROV [2]). Since the end of the 1980's, DO has been widely and successfully used in craniofacial surgery for different purposes (KARP et al. [3], McCARTHY et al. [4]). The indications of this technique are mainly congenital

malformations and craniofacial traumas. For the first category of indications, internal devices are generally used to achieve the distraction osteogenesis. Concerning traumas with significant bone defects, external bone transport devices are often indicated (LABBÉ et al. [5]).

Bone distraction forces in maxillofacial surgery have already been studied in the past in human mandible (ROBINSON et al. [6]). Unidirectional screw-bolt type devices were used and the distraction forces were determined from the activation torque. Patients were undergoing unilateral or bilateral DO following congenital diseases. This study was aimed at measuring the maximal distraction forces at each increment with no consideration of the bone regenerate time-dependent behavior.

* Corresponding author: Paul Lipinski, Laboratory of Mechanics, Biomechanics, Polymers and Structures, Ecole Nationale d'Ingénieurs de Metz, 1 route d'Ars Laquenexy CS 65820, 57078 Metz Cedex, France. Tel.: 33 3 87 34 42 63, 33 3 87 34 69 35, e-mail: lipinski@enim.fr

Received: March 26th, 2012

Accepted for publication: September 28th, 2012

LOBOA et al. [7] measured, by *ex vivo* experiments on a rat model, the tension forces and displacements and quantified the stresses and strains occurring throughout mandibular distraction. In addition, several studies explored bone transport forces in lower limb DO. Most of them attempted to determine the link existing between forces and clinical issue (ARONSON [8]; ARONSON and HARP [9]; BRUNNER et al. [10]). Others tried to determine the origin of these forces (GARDNER et al. [11]; GARDNER et al. [12]; HOLLIS et al. [13]; WOLFSON et al. [14]; YOUNGER et al. [15]).

The purpose of this work was to determine the evolving transport forces of bone regenerate during the early phases of human mandibular DO.

2. Materials and Methods

2.1. Patient and treatment planning

One 37-year-old male with multi-tissular facial defect from a gunshot trauma was considered in this study. The patient was undergoing DO reconstruction for a 60 mm defect of the mandible and attached soft tissues, including skin cover. An external custom-made bone transport device (DEOS, OBL, France, see figure 1a) was used. After surgery, a latency period of six days was observed. The distraction system was activated twice a day at a mean daily rate of 1 mm.

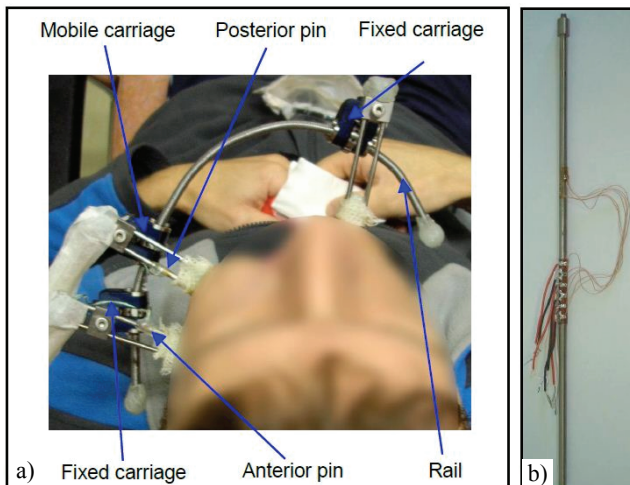


Fig. 1. Views of the whole custom-made bone transport device (a) and pin equipped with strain gauges (b)

The patient gave full specific consent and the research protocol received approval by a local ethic

committee. The measurement procedure did not interfere with the treatment planning.

The apparatus includes two fixed carriages used to anchor the device on bone and at least one mobile one for bone segment transport. Pins are clamped to each carriage to fix the device on bone using plate implants. The mobile carriage is displaced thanks to an endless screw – nut set. The nuts are incorporated into the carriages. The endless screw that can be referred to as the rail has for particularity to be custom-bent for each patient to optimize the bone path. In the case presented here, the treatment consisted in a bifocal DO with one mobile carriage (LABBÉ et al. [5]).

2.2. Measurement equipment

To determine distraction forces during the activation process, two pins of the distraction device were equipped with strain gauges (Vishay USA EA-06-015LA-120), namely the posterior pin of the mobile carriage and the anterior pin of the fixed one. As distraction forces are relatively moderate compared to the device strength, it was necessary to identify a part of the device undergoing significant deformations to ensure precision of the measurements. The flexible pins appeared to be good candidates. They are submitted to significant bending stresses and play the role of reservoirs of elastic energy enabling continuous bone distraction. They were chosen for the placement of the gauges. Besides, the distraction device had to be sterilized before surgery and thus endured exposition during 20 minutes to steam at a temperature of 134 °C under the absolute pressure of 200 kPa. The measuring gear was chosen and set up in consequence.

Since it is impossible to glue the strain gauges after the DEOS set up, the mounting position was foreseen with the surgeons' help using CT-scan files exploited in a CAD software package (3-matic, Materialise Software, Belgium). An example of a distraction pin equipped with strain gauges is shown in figure 1b.

2.3. Modus operandi

Strain values were recorded by means of a data acquisition system (SCXI, National Instruments, USA) connected to a PC computer. The acquisition was done using a LabView program (National Instruments, USA). Records started about one minute be-

fore the activation of the bone transport device and ended about one hour later.

The activation in the first week was conducted during hospital stay for clinical surveillance and patient's education. The recording procedure described above was repeated for each distraction increment during this week. The patient was discharged home at the end of the week and was asked to keep activating the device himself twice a day. Two additional measurements were done during check-ups of the patient at post-operative weeks 4 and 6.

2.4. Data post processing

Figure 2 illustrates a typical geometric configuration of the DEOS during DO. To develop the formulae used in data post processing, a local orthogonal coordinate system is attached to each carriage. Its x -axis is oriented towards the regenerate and is contained in the rail plane. The y -axis is parallel to the pins clamped to the carriage considered and points the bone. The farthest pin from the regenerate is named "pin 1". The following geometrical parameters are used to describe such a configuration:

$$\begin{aligned}
 F &= \frac{w}{(\Delta l^2 + a^2)} \left[-2a \left(\frac{B_1}{l_1 - 2g_1} + \frac{B_2}{l_2 - 2g_2} + \frac{\theta E_1 I_1}{l_1(l_1 - 2g_1)} + \frac{\theta E_2 I_2}{l_2(l_2 - 2g_2)} \right) + \Delta l(T_1 + T_2) \right] \\
 S &= \frac{w}{(\Delta l^2 + a^2)} \left[\Delta l \left(\frac{2(B_1 l_1 + E_1 I_1 \theta)}{l_1(l_1 - 2g_1)} + \frac{2(B_2 l_2 + E_2 I_2 \theta)}{l_2(l_2 - 2g_2)} \right) + a(T_1 + T_2) \right] \\
 C &= -T_1 a - (T_1 + T_2) \left(b \frac{a}{w} - e \frac{\Delta l}{w} \right) + \frac{l_1^2 B_1 + 2g_1 E_1 I_1 \theta}{l_1(l_1 - 2g_1)} + \frac{l_2^2 B_2 + 2g_2 E_2 I_2 \theta}{l_2(l_2 - 2g_2)} \\
 &\quad - \frac{2(l_2 w + b \Delta l + ea)}{w(l_1 - 2g_1)} \left(B_1 + \frac{E_1 I_1}{l_1} \theta \right) - \frac{2(l_2 w + b \Delta l + ea)}{w(l_2 - 2g_2)} \left(B_2 + \frac{E_2 I_2}{l_2} \theta \right)
 \end{aligned} \tag{2}$$

- l_1 and l_2 are the working lengths of pins,
- a indicates the distance between the two pin axes of the same carriage,
- ω is the angle orienting the instantaneous distraction direction with respect to the coordinate system,
- g_1 and g_2 locate the pin section comprising gauges with respect to the holder,

- $2e$ defines a mean value of the bone segment thickness,
- b is the distance between pin 2 extremity and the regenerate section,
- w is the distance between pins' extremities.

Let δ be the displacement increment imposed to the mobile carriage (typically 0.5 mm) tangent to the rail. This displacement causes deformation of the pins and generates the following distraction forces acting on callus: \vec{F}_c , \vec{S}_c , \vec{C}_c , i.e., the tension force, shear force and bending moment, respectively. The system is sketched in figure 2 in initial and deformed configurations.

By the action-reaction principle, the forces applied to the transported bone segment are defined by:

$$\vec{F} = -\vec{F}_c, \quad \vec{S} = -\vec{S}_c, \quad \vec{C} = -\vec{C}_c. \tag{1}$$

To determine these actions, the equilibrium of the system composed of two pins and the transported bone segment was analyzed. The details of this analysis are provided in Appendix A.

In the general case sketched in figure 2, the solution of the above problem is given by:

where:

$$\theta = \frac{1}{a} \left(\frac{T_2 l_2}{E_2 A_2} - \frac{T_1 l_1}{E_1 A_1} \right) \tag{3}$$

and

- T_1 and T_2 are the internal tension forces,
- E_1 and E_2 are the pins' Young's moduli,

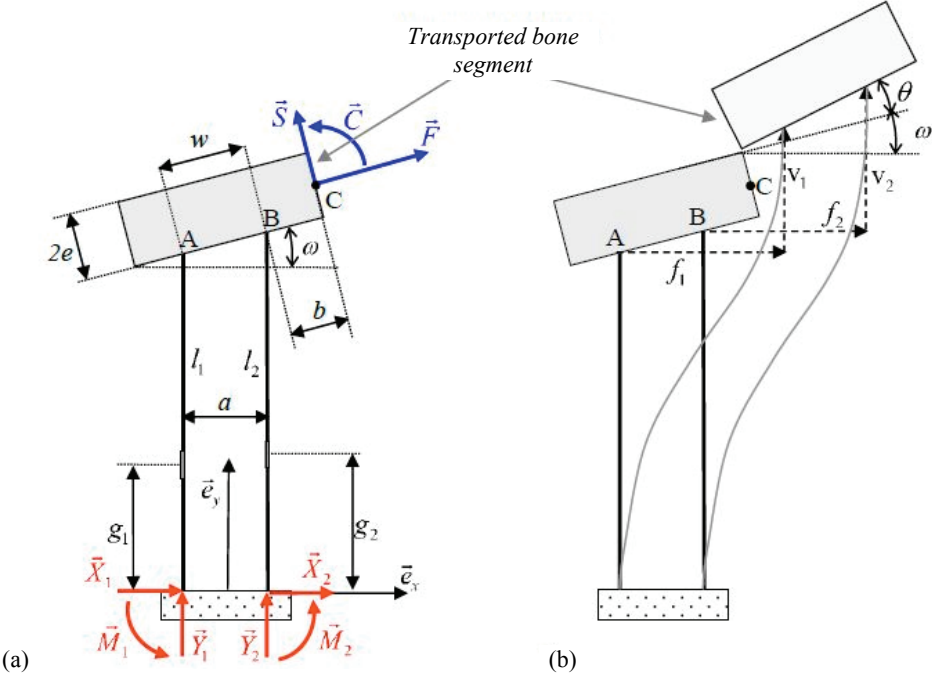


Fig. 2. Diagram of static analysis parameters: (a) initial configuration, (b) deformed configuration

- A_1 and A_2 are the pin sections,
 - B_1 and B_2 are the internal bending moments,
 - I_1 and I_2 are the moments of inertia,
- for pins 1 and 2, respectively.

In the case of “perfectly mounted” device defined by the following relationships, with i taking values 1 and 2:

$$\begin{aligned} l_i &= l; \quad w = a; \quad g_i = g; \\ A_i &= A; \quad I_i = I; \quad E_i = E, \end{aligned} \quad (4)$$

the above solution of equilibrium problem takes much more compact form:

$$\left. \begin{aligned} S_i &= T_1 + T_2 \\ F &= -\frac{4}{l-2g} \left[B_2 + \frac{I}{Aa} (T_2 - T_1) \right] \\ C &= -\frac{2B_2(l+2e)}{l-2g} + (T_2 - T_1) \frac{4I(g-l-e)}{Aa(l-2g)} - T_1(a+b) - T_2b \end{aligned} \right\} \quad (5)$$

Moreover, it is assumed in the present work that the moment C can be neglected. This hypothesis is well verified here, as the distance between the pins is large enough compared to their diameter, i.e., $a \gg d$. In that case, the measurement of internal actions of one pin per carriage is sufficient to determine the distraction forces F and S . System (5) becomes:

$$\left. \begin{aligned} S &= \frac{a^2 A(l-2g)T_2 - 2aA(2e+l)B_2 - 8I(l+e-g)T_2}{aA(l-2g)(a+b) - 4I(l+e-g)} \\ F &= \frac{8B_2I - 4Aa(a+b)B_2 - 4I(a+2b)T_2}{aA(l-2g)(a+b) - 4I(l+e-g)} \end{aligned} \right\} \quad (6)$$

The regenerate interface displacement can be calculated using:

$$\vec{d}(C) = (f_2 - e\theta)\vec{e}_x = (v_2 + b\theta)\vec{e}_y \quad (7)$$

with

$$\left. \begin{aligned} v_2 &= \frac{T_2 l}{E A} \\ f_2 &= \frac{l-3g}{l-2g} \frac{(2T_2 - S)}{EA} \frac{l^2}{3a} - \frac{b_2 l^3}{6EI(l-2g)} \end{aligned} \right\} \quad (8)$$

corresponding respectively to the elongation and deflection of the second pin, see figure 2.

The rotation angle θ is given by:

$$\theta = \frac{l(2T_2 - S)}{EAa}. \quad (9)$$

The internal actions T_i and B_i produce strains ε_1 , ε_2 and ε_3 , at gauges G_1 , G_2 , and G_3 , respectively. By measuring these strains, one can find the internal actions as well as the unknown angle φ defining the relative orientation of gauge G_1 with respect to the

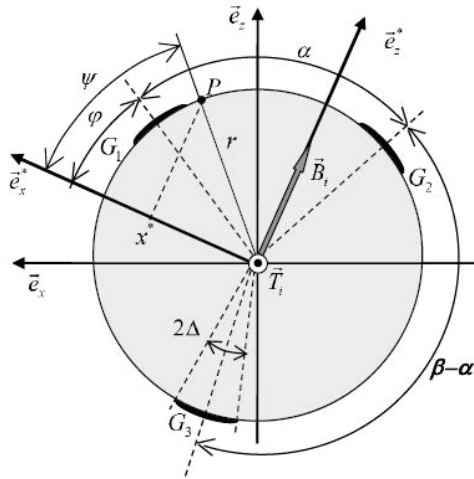


Fig. 3. Gauges positioning parameters

bending plane. As illustrated in figure 3, the orientations of gauges G_2 and G_3 with respect to gauge G_1 were defined by the angles α and β , respectively. The following relations detailed in Appendix B are valid:

$$\left. \begin{aligned} T_i &= A_i E_i \varepsilon_T \\ B_i &= \frac{2E_i I_i}{d} \varepsilon_{B \max} \end{aligned} \right\} \quad (10)$$

where the strain components due to the tension force and bending moment are given by:

$$\varepsilon_T = \frac{\varepsilon_1 \sin(\beta - \alpha) - \varepsilon_2 \sin \beta + \varepsilon_3 \sin \alpha}{\sin \alpha - \sin \beta + \sin(\beta - \alpha)}, \quad (11)$$

$$\varepsilon_{B \max} = \pm \frac{(\varepsilon_2 - \varepsilon_1) \sin \beta - (\varepsilon_3 - \varepsilon_1) \sin \alpha}{\sin \alpha - \sin \beta + \sin(\beta - \alpha)} \times \sqrt{(\tan^2 \varphi + 1)} \frac{\Delta}{\sin \Delta}, \quad (12)$$

$$\text{with } \tan \varphi = \frac{\varepsilon_2 - \varepsilon_3 + (\varepsilon_3 - \varepsilon_1) \cos \alpha + (\varepsilon_1 - \varepsilon_2) \cos \beta}{(\varepsilon_3 - \varepsilon_1) \sin \alpha + (\varepsilon_1 - \varepsilon_2) \sin \beta}.$$

Δ is called the gauge angle and is defined by the gauge width p and pin diameter d :

$$\Delta = \frac{p}{d}. \quad (13)$$

The gauge length is denoted by λ . This procedure was automated and applied to all records through a Fortran program. The values of various parameters corresponding to the DEOS and geometric characteristics of the gauges are summarized in table 1. This table also specifies the initial length l_c^0 and average

thickness of bone regenerate e as well as its section A_c and quadratic moment I_c estimated thanks to the pre-distraction CT scan exam of the mandible.

Table 1. Values of the different parameters used

	Parameter	Unit	Posterior mobile pin	Anterior fixed pin
DEOS	a	mm	10	
	b	mm	5	20
	d	mm	2.5	
	g	mm	23	19
	l	mm	72	66
	E	MPa	135,000	
Gauges	λ	mm	0.51	
	p	mm	0.51	
	α	$^\circ$	90	90
	β	$^\circ$	225	225
Bone regenerate	e	mm	5	
	l_c^0	mm	1.5	
	A_c	mm^2	285	
	I_c	mm^4	3780	

The forces acting on each side of the distracted bone regenerate were determined considering separately the strain measurements on the fixed anterior and mobile posterior pins. This enabled us to plot the curves of bone regenerate loads versus time and to estimate the quality of our results by comparing the actions computed from the fixed and mobile sides.

3. Results

3.1. Strain measurements

The above-mentioned procedure enabled us to create a database containing nine strain records. Although the device was manipulated by the patient with care, some parts of the measuring system were progressively damaged making the last two records (weeks 4 and 6) incomplete or mistrustful. For these reasons they are not reported here. Finally, only six of them permitted the calculation of internal actions of the pins, callus force and callus extension as the data concerning activation 6 were unusable. Besides, for various reasons, during the first and second activations, the strains of only one pin were exploitable, namely on mobile carriage for the first activation and on fixed carriage for the second one.

The duration of each record (t_{end}), depending on the patient's convenience, is summarized in table 2 for the six successfully performed records. All data that

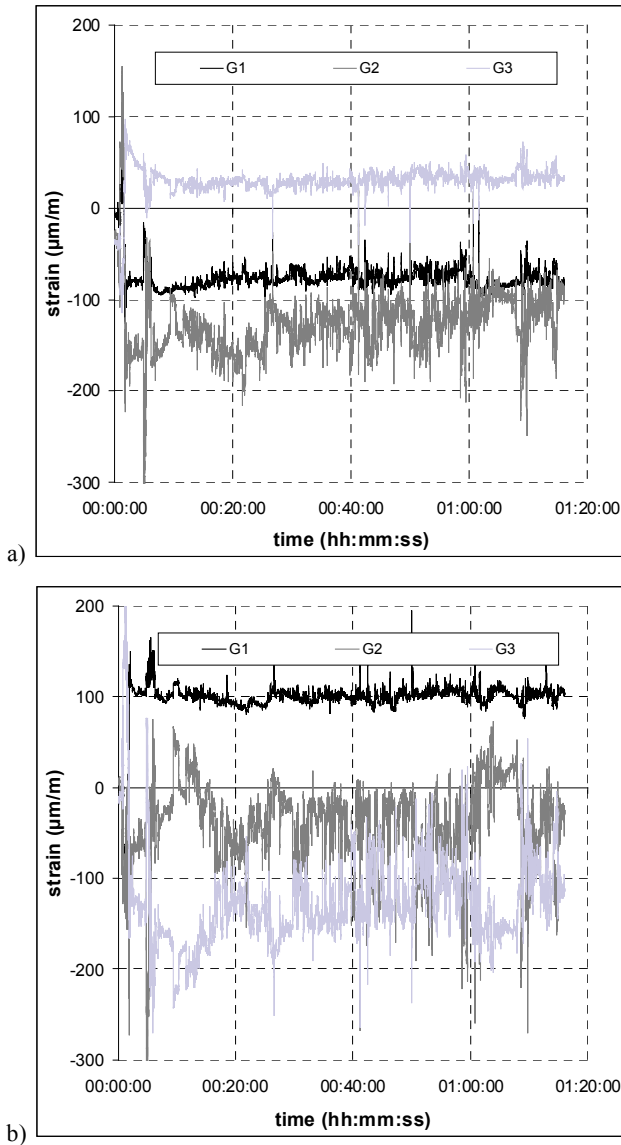


Fig. 4. Longitudinal strains versus time for the 7th activation:
(a) posterior mobile pin, (b) anterior fixed pin

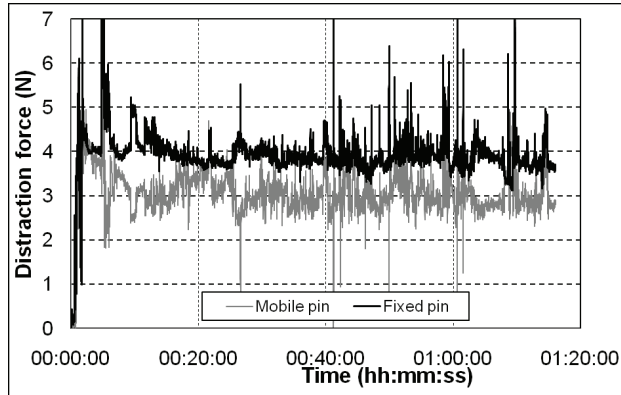


Fig. 5. Distraction forces versus time for the 7th activation obtained from the posterior mobile and anterior fixed pins

could be treated led to similar curves. It must also be noted that all the values of the recorded strains had

returned to zero before the beginning of a new distraction, indicating a complete unloading of the distraction device after a twelve-hour period. For all these reasons, records are only presented for a typical activation, i.e., the one done on the fourth day morning (seventh activation).

Table 2. Record duration

Activation number	1	2	3	4	5	6	7
t_{end} [s]	93	400	5400	1130	1100	1090	4400

The strains arising in mobile posterior and fixed anterior pins are illustrated in figure 4. It can be noted that records are quite perturbed due to patient's activities. The mean measured strain magnitude is around 100 $\mu\text{m}/\text{m}$. Comparing with the precision of the gauges (1 μm), these values are significant and confirm the good choice of their positioning. The records are fairly dissimilar for both pins as their angular orientations defined by angle φ are different. The procedure presented above enabled us to estimate these angles. The values obtained are quite the same for all six records and equal -40° and 80° for the posterior mobile and anterior fixed pins, respectively. These results are not illustrated in this paper.

3.2. Tension and shear distraction forces

Figure 5 shows the evolution of the tension distraction force F obtained from the posterior mobile pin and the anterior fixed one. The results show the same tendency for both curves confirming the validity of our approach. Two distinct phases can be clearly identified: the activation phase where the force rapidly grows up from zero to its maximal value and the relaxation one where a slow decrease of the force is observed. Ignoring noise, one can estimate the maximal value to be approximately 4.6 N for both pins. After 75 minutes the distraction force has been reduced to about 2.8 N for the mobile pin and 3.6 N for the fixed one, corresponding respectively to a loss of 38% and 20% of their initial values.

The shear forces S are not illustrated in this work as they do not exceed 2 N during the whole distraction process. The maximum value is obtained at the end of each activation.

3.3. Deflection of the pins and callus elongation

The deflection of both pins and the consequential callus extension are depicted in figure 6. The deflection curves are very similar during the whole distraction process. At the end of activation phase, i.e., after around 10 seconds, the sum of these deflections is close to 0.5 mm. This value corresponds to the increment of displacement imposed on the mobile carriage. During the remaining measurement time, the deflections decrease monotonically to reach a value of approximately 0.18 mm.

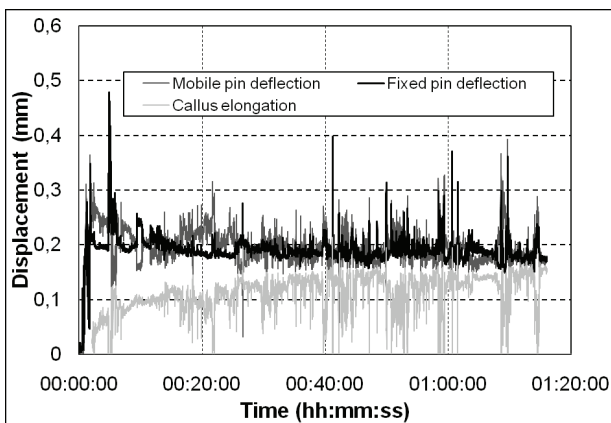


Fig. 6. Deflection of posterior mobile pin, anterior fixed one and callus lengthening versus time for the 7th activation

The regenerative extension is obtained using the following expression:

$$u = \delta - f_1 - f_2.$$

This expression is valid only after the end of activation. The evolution of u is monotonically increasing during distraction. After 75 minutes of distraction, a regenerative lengthening of 0.17 mm is obtained.

3.4. Evolution of distraction force versus regenerative extension

The evolution of the distraction force as a function of the callus lengthening is illustrated in figure 7 for all valid activations. The number of points depends on the record duration (see table 2). The time instant for which the maximal value of distraction force is reached is called peak time and denoted t_{peak} . For all measurements, the forces and corresponding extension values at t_{peak} and t_{end} have been estimated. Besides, if

available, these values were also estimated at $t_{peak} + 60$, $t_{peak} + 180$, $t_{peak} + 600$, $t_{peak} + 1800$. It clearly appears in figure 7 that all data are consistent. The slope of the fitting curve provides the stiffness of the distraction device. This stiffness is estimated to be 10.03 N/mm. The average peak distraction force remains roughly constant for all activations and can be evaluated to 4.69 N.

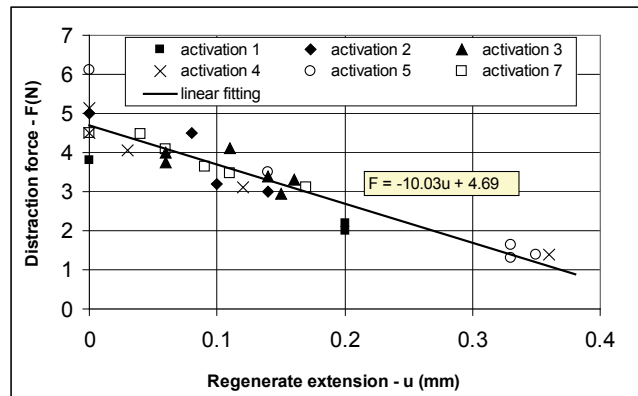


Fig. 7. Distraction force versus callus lengthening

4. Discussion

4.1. Strain measurements

The slightly noisy character of the signals of the gauges (cf. figure 4) could not be avoided regarding the measurement conditions. As the strain magnitude is quite small (around 100 $\mu\text{m/m}$), high sensitivity was required. Besides, the device inertia is important due to the mass of the assembly suspended to long pins. Consequently, small motions of the patient's head engendered perturbations of the recorded strain values. Even if the patient was asked to stay immobile, some motions such as those due to deglutition could not be avoided leading to a noisy response. It can also be noted that the records obtained were particularly perturbed during the activation phase when the distraction device was handled by the surgeon or patient. This testifies to its high sensitivity.

4.2. Distraction force

All curves of distraction force versus time exhibit three distinct phases illustrated by figure 5. The first phase corresponds to the application of the desired mobile carriage displacement of 0.5 mm. During this

phase, as the bone regenerate opposes to the motion of the mobile bone segment, the distraction force increases rapidly to reach its maximal value at the end of activation, typically after 10 to 60 seconds. It can be seen in figure 7 that this maximal value is quasi independent of the activation number, i.e., of the current callus length which expanded about 0.5 mm per activation. This indicates a viscous behavior of the regenerate. Indeed, the viscosity impedes instantaneous callus lengthening during relatively rapid activation phases. During this phase almost the whole activation energy is stored in the DO device mainly inducing a pure bending of flexible pins. As the resulting deflection of these pins is roughly constant for all activations, a relatively stable value of the maximal distraction force is obtained. The scatter of maximal distraction force observed in figure 7 can partially be attributed to the various activation time-spans.

The second phase is characterized by an exponential decrease of the distraction force typically during 300 to 500 seconds. This fast force drop is due to the callus viscoelastic relaxation process. This phenomenon was accompanied by a regenerate lengthening of about 0.1 mm, see figure 6.

The third phase is distinguished by a continuous decrease of the distraction force in a nearly linear manner. On average, this force diminished from 3.7 to 3.2 N during a period of 4000 s and was accompanied by an additional callus extension of about 0.05 mm. It clearly appears that such an evolution of the force is due to another viscous mechanism of regenerate lengthening characterized by a relaxation time much longer than that of the second phase.

The maximal or peak value of distraction forces obtained in this work is surprisingly feeble (≈ 5 N) compared to the one obtained in the unique *in vivo* study interested in early distraction force measurements of human mandible (ROBINSON et al. [6]). The same rate and rhythm as in our analyses were applied for 8 patients and led to an average peak distraction force value of 35.6 ± 13.4 N.

At least two reasons allow explaining these differences. First, for all patients treated by Robinson et al., relatively stiff distraction devices were used. Therefore, the whole imposed displacement was practically instantaneously applied to the regenerate. So, the lengthened tissue underwent a “relaxation test” with imposed strain step. This type of loading generates high reaction of the viscous tissues as was observed by many authors. The DEOS used in our analysis is characterized by low stiffness (≈ 10 N/mm) and high stored energy. Immediately after a relatively slow activation period, the callus extension for all records

did not exceed 0.05 mm for the displacement increment of 0.5 mm leading to a much smaller strain step and consequently to the feeble value of peak distraction force. Moreover, in our case, during the rest of the distraction cycle, the tissue underwent a creep like loading with progressively diminishing applied force. Finally, in contrast to the study of ROBINSON et al. [6] concerning the treatment of indications such as mandibular hypoplasia, the soft tissues of our patient were greatly destroyed by a bullet and did not participate in resistance to the lengthening.

In their experimental analysis with a rat model of mandible distraction in *ex vivo* conditions, LOBOA et al. [7] determined the average distraction force peaks ranging from 0.3 N for an end latency specimen to 4.1 N for post-operative day 13. For the purpose of comparison with our study, two additional differences have to be pointed. The rat's callus cross-section area was approximately 10 times smaller than the human one and the rate of distraction was 0.25 mm twice daily. The important stiffness of the *ex vivo* testing apparatus illustrated in figure 1C of [7] as well as the short loading time of 0.5 s led to a relaxation type loading. The mean value of peak force on 2 and 5 distraction days, well corresponding to our tests, is about 0.65 N. Multiplying this value by the ratio of the cross-section areas, a force of 6.5 N is obtained which is 30% higher than the value of 4.6 N determined in our study. This difference can probably be attributed to the much higher load rate applied in the tests by LOBOA et al. [7]. The soft tissues were eliminated in Loboa et al.'s experiments.

These two comparisons clearly suggest that the soft tissues bear a large part of lengthening load. In the literature concerning lower limb distraction, only 25% of this load is generally attributed to the soft tissue resistance; ARONSON [8]; ARONSON and HARP [9]; BRUNNER et al. [10]; Younger et al. [15], Hollis et al. [13]. This percentage seems to be highly underestimated. Our results support the WOLFSON'S et al. [14] and GARDNER'S et al. [11] thesis of a crucial role of the soft tissues in the limb distraction resistance phenomenon.

References

- [1] ILIZAROV G.A., *The Tension-Stress Effect on the Genesis and Growth of Tissues. Part II. The Influence of the Rate and Frequency of Distraction*, Clin. Orthop. Relat. Res., 1989, 239, 263–285.
- [2] ILIZAROV G.A., *The principles of the Ilizarov method*, Bull. Hosp. Jt Dis. Orthop. Inst., 1988, 48, 1–11.
- [3] KARP N.S., THORNE C.H., McCARTHY J.G., SISSONS H.A., *Bone lengthening in the craniofacial skeleton*, Ann. Plas. Surg., 1990, 24, 231–237.

- [4] McCARTHY J.G., SCHREIBER J., KARP N., THORNE C.H., GRAYSON B.H., *Lengthening the human mandible by gradual distraction*, Plast. Reconstr. Surg., 1992, 89, 1–8.
- [5] LABBÉ D., NICOLAS J., KALUZINSKI E., SOUBEYRAND E., SABIN P., COMPÈRE J.F., BÉNATEAU H., *Gunshot Wounds: Reconstruction of the lower face by osteogenic distraction*, Plast. Reconstr. Surg., 2005, 116, 1596–1603.
- [6] ROBINSON R.C., O’NEAL B.J., ROBINSON G.H., *Mandibular distraction force: laboratory data and clinical correlation*, J. Oral. Maxil. Surg., 2001, 59, 539–544.
- [7] LOBOA E.G., FANG T.D., WARREN S.M., LINDSEY D.P., FONG K.D., LONGAKER M.T., CARTER D.R., *Mechanobiology of mandibular distraction osteogenesis: experimental analyses with a rat model*, Bone, 2004, 34, 336–343.
- [8] ARONSON J., *Experimental and clinical experience with distraction osteogenesis*, Cleft Palate-Cran. J., 1994, 31, 473–481.
- [9] ARONSON J., HARP J.H., *Mechanical forces as predictors of healing during tibial lengthening by distraction osteogenesis*, Clin. Orthop. Relat. Res., 1994, 301, 73–79.
- [10] BRUNNER U.H., CORDEY J., SCHWEIBERER L., PERREN S.M., *Force required for bone segment transport in the treatment of large bone defects using medullary nail fixation*, Clin. Orthop. Relat. Res., 1994, 301, 147–155.
- [11] GARDNER T.N., EVANS M., SIMPSON A.H., KENWRIGHT J., *A method of examining the magnitude and origin of soft and hard tissue forces resisting limb-lengthening*, J. Biomed. Eng., 1997, 19, 405–411.
- [12] GARDNER T.N., EVANS M., SIMPSON H., KENWRIGHT J., *Force-displacement behaviour of biological tissue during distraction osteogenesis*, Med. Eng. Phys., 1998, 20, 708–715.
- [13] HOLLIS J.M., ARONSON J., HOFMANN O.E., *Differential loads in tissues during limb lengthening*, Trans. Orthop. Res. Soc., 1992, 14, 388–389.
- [14] WOLFSON N., HEARN T.C., THOMASON J.J., ARMSTRONG P.F., *Force and stiffness changes during Ilizarov leg lengthening*, Clin. Orthop. Relat. Res., 1990, 250, 58–60.
- [15] YOUNGER A.S.E., MACKENZIE W.G., MORRISON J.B., *Femoral forces during limb lengthening in children*, Clin. Orthop. Relat. Res., 1994, 301, 55–63.

Appendix A

The obvious geometrical relations are considered:

$$\sin \omega = \frac{l_2 - l_1}{w} = \frac{\Delta l}{w}, \quad (\text{A1})$$

$$\cos \omega = \frac{a}{w}. \quad (\text{A2})$$

Let X_1 , Y_1 , M_1 and X_2 , Y_2 , M_2 be the reactions appearing at holders (see figure 3). The problem being plane, three equilibrium equations may be written. They correspond to the projection of forces

on x and y -axes and the projection of moments on z -axis:

$$\left. \begin{aligned} X_1 + X_2 + F \cos \omega - S \sin \omega &= 0 \\ Y_1 + Y_2 + F \sin \omega + S \cos \omega &= 0 \\ C + M_1 + M_2 + (X_1 + X_2)(l_2 + b \sin \omega + e \cos \omega) \\ - Y_1 a - (Y_1 + Y_2)(b \cos \omega - e \sin \omega) &= 0 \end{aligned} \right\} \quad (\text{A3})$$

Referring to equations (A1) and (A2), system (A3) can be solved to express the unknown forces acting on transported bone segment as a function of reactions applied to pins:

$$\left. \begin{aligned} F &= -\frac{w}{(\Delta l^2 + a^2)} [a(X_1 + X_2) + \Delta l(Y_1 + Y_2)] \\ S &= -\frac{w}{(\Delta l^2 + a^2)} [\Delta l(X_1 + X_2) - a(Y_1 + Y_2)] \\ C &= -M_1 - M_2 (X_1 + X_2) \left(l_2 + b \frac{\Delta l}{w} + e \frac{a}{w} \right) \\ &+ Y_1 a + (Y_1 + Y_2) \left(b \frac{a}{w} - e \frac{\Delta l}{w} \right) \end{aligned} \right\} \quad (\text{A4})$$

Each pin is considered as a beam clamped by the holder. Thus, the well-known solution of the cantilever beam problem may be exploited to determine these reactions experimentally. Let $T_i(y)$ and $B_i(y)$ be the internal tension forces and $B_i(y)$ and $B_i(y)$ the resultant internal bending moments acting in a given pin section defined by the y coordinate. These internal actions can be expressed as a function of the problem reactions:

$$\begin{aligned} T_i(y) &= -Y_i, \\ B_i(y) &= -yX_i - M_i. \end{aligned} \quad (\text{A5})$$

On the other hand, they can be deduced from the deformation of the pins. This point is addressed later on. For the moment, it is supposed that these internal actions are known at the locations $y = g_i$, so the following relations hold:

$$\begin{aligned} Y_i &= -T_i, \\ M_i &= -g_i X_i - B_i, \end{aligned} \quad (\text{A6})$$

where $B_i = B_i(g_i)$. These four equations have to be completed by two kinematic relations. The

transported bone segment can be supposed perfectly rigid in comparison to the pins and callus stiffness. So, the distance between any two points of the segment is preserved and its rotation angle, around an instantaneous rotation axis \vec{k} , is unique during motion. If this rotation angle is small ($\theta \ll 1$), the following relation holds for any two points of a rigid body:

$$\vec{u}(B) = \vec{u}(A) + \theta \vec{k} \wedge \overrightarrow{AB}. \quad (\text{A7})$$

Let f_i , v_i and θ_i be the deflection, elongation and rotation of the i -th pin extremity fixed to the bone segment (points A and B in figure 2). It follows from the above hypothesis and expression (A7) specified for $\vec{k} = \vec{e}_z$ that:

$$\begin{aligned} \theta_1 &= \theta_2 = \theta \\ f_2 \vec{e}_x + v_2 \vec{e}_y &= f_1 \vec{e}_x + v_1 \vec{e}_y + \theta \vec{e}_z \wedge (a \vec{e}_x + \Delta l \vec{e}_y) \end{aligned}$$

which leads to:

$$\left. \begin{aligned} \theta_1 &= \theta_2 = \theta \\ f_2 &= f_1 - \Delta l \theta \\ v_1 + \theta a &= v_2 \end{aligned} \right\} \quad (\text{A8})$$

On the other hand, the following results hold for the cantilever beam problem:

$$\left. \begin{aligned} F &= \frac{w}{(\Delta l^2 + a^2)} \left[-2a \left(\frac{B_1}{l_1 - 2g_1} + \frac{B_2}{l_2 - 2g_2} \right) + \frac{\theta E_1 I_1}{l_1(l_1 - 2g_1)} + \frac{\theta E_2 I_2}{l_2(l_2 - 2g_2)} + \Delta l(T_1 + T_2) \right] \\ S &= \frac{w}{(\Delta l^2 + a^2)} \left[\Delta l \left(\frac{2(B_1 l_1 + E_1 I_1 \theta)}{l_1(l_1 - 2g_1)} + \frac{2(B_2 l_2 + E_2 I_2 \theta)}{l_2(l_2 - 2g_2)} \right) + a(T_1 + T_2) \right] \\ C &= -T_1 a - (T_1 + T_2) \left(b \frac{a}{w} - e \frac{\Delta l}{w} \right) + \frac{l_1^2 B_1 + 2g_1 E_1 I_1 \theta}{l_1(l_1 - 2g_1)} + \frac{l_2^2 B_2 + 2g_2 E_2 I_2 \theta}{l_2(l_2 - 2g_2)} \\ &\quad - \frac{2(l_2 w + b \Delta l + ea)}{w(l_1 - 2g_1)} \left(B_1 + \frac{E_1 I_1}{l_1} \theta \right) - \frac{2(l_2 w + b \Delta l + ea)}{w(l_2 - 2g_2)} \left(B_2 + \frac{E_2 I_2}{l_2} \theta \right) \end{aligned} \right\} \quad (\text{A12})$$

where E_i , A_i and I_i are Young's modulus, cross-section area and inertia of pin (i), respectively. Using (A9), systems (A8) and (A6) can be solved with respect to the unknown reactions:

$$\left. \begin{aligned} Y_i &= -T_i \\ X_i &= \frac{2}{l_i - 2g_i} \left(B_i + \frac{E_i I_i}{l_i} \theta \right) \\ M_i &= -\frac{1}{l_i - 2g_i} \left(l_i B_i + \frac{2g_i E_i I_i}{l_i} \theta \right) \end{aligned} \right\} \quad (\text{A10})$$

where

$$\theta = \frac{1}{a} \left(\frac{T_2 l_2}{E_2 A_2} - \frac{T_1 l_1}{E_1 A_1} \right). \quad (\text{A11})$$

Substitution of (A10) into (A4) leads to the problem solution:

Appendix B

Two coordinate systems are considered, see figure 3. The first one ($O; \vec{e}_x, \vec{e}_y, \vec{e}_z$) is attached to the pin and has been introduced before. The second one ($O; \vec{e}_x^*, \vec{e}_y^*, \vec{e}_z^*$) corresponds to the bending plane ($\vec{B}_i = B_i \vec{e}_z^*$) and is defined by angle φ with respect to the first gauge G_1 . Assuming that the strain field in a pin section considered is mainly due to the tension force T_i and bending moment B_i , the corresponding strain components ε_T and ε_B exerted at point P are given by:

$$\varepsilon_T = \frac{T_i}{A_i E_i}, \quad (B1)$$

$$\varepsilon_B(x^*) = \frac{B_i}{I_i E_i} x^*.$$

This last strain can be expressed using the angle ψ positioning the current point P with respect to \vec{e}_x^* .

$$\varepsilon_B(\psi) = \frac{B_i}{I_i E_i} \frac{d_i}{2} \cos \psi = \varepsilon_{B\max} \cos \psi \quad (B2)$$

where

$$\varepsilon_{B\max} = \frac{B_i}{I_i E_i} \frac{d_i}{2}. \quad (B3)$$

The total strain is obtained by addition of (B1) and (B2):

$$\varepsilon(\psi) = \varepsilon_T + \varepsilon_{B\max} \cos \psi. \quad (B4)$$

Let p be the width of any gauge glued on a pin of diameter d_i . When p is comparable with d_i , the strain measured by the gauge can be significantly different from that corresponding to the position of its centre. Let Δ be the gauge angle such that:

$$\Delta = \frac{p}{d}. \quad (B5)$$

The average strains recorded by three gauges are given by:

$$\left. \begin{aligned} \varepsilon_1 &= \frac{1}{2\Delta} \int_{\varphi-\Delta}^{\varphi+\Delta} (\varepsilon_T + \varepsilon_{B\max} \cos \psi) d\psi \\ &= \varepsilon_T + \frac{\varepsilon_{B\max}}{2\Delta} \int_{\varphi-\Delta}^{\varphi+\Delta} \cos \psi d\psi \\ \varepsilon_2 &= \frac{1}{2\Delta} \int_{\varphi+\alpha-\Delta}^{\varphi+\alpha+\Delta} (\varepsilon_T + \varepsilon_{B\max} \cos \psi) d\psi \\ &= \varepsilon_T + \frac{\varepsilon_{B\max}}{2\Delta} \int_{\varphi+\alpha-\Delta}^{\varphi+\alpha+\Delta} \cos \psi d\psi \\ \varepsilon_3 &= \frac{1}{2\Delta} \int_{\varphi+\beta-\Delta}^{\varphi+\beta+\Delta} (\varepsilon_T + \varepsilon_{B\max} \cos \psi) d\psi \\ &= \varepsilon_T + \frac{\varepsilon_{B\max}}{2\Delta} \int_{\varphi+\beta-\Delta}^{\varphi+\beta+\Delta} \cos \psi d\psi \end{aligned} \right\} \quad (B6)$$

where angles α and β locate gauges G_2 and G_3 with respect to gauge G_1 .

After integration (B6) becomes:

$$\left. \begin{aligned} \varepsilon_1 &= \varepsilon_T + \varepsilon_{B\max} \frac{\sin \Delta}{\Delta} \cos \varphi \\ \varepsilon_2 &= \varepsilon_T + \varepsilon_{B\max} \frac{\sin \Delta}{\Delta} \cos(\varphi + \alpha) \\ \varepsilon_3 &= \varepsilon_T + \varepsilon_{B\max} \frac{\sin \Delta}{\Delta} \cos(\varphi + \beta) \end{aligned} \right\} \quad (B7)$$

This system has to be solved with respect to φ , ε_T and $\varepsilon_{B\max}$. After some transformations one gets:

$$\varepsilon_T = \frac{\varepsilon_1 \sin(\beta - \alpha) - \varepsilon_2 \sin \beta + \varepsilon_3 \sin \alpha}{\sin \alpha - \sin \beta + \sin(\beta - \alpha)}. \quad (B8)$$

This result enables determination of angle φ :

$$\tan \varphi = \frac{\varepsilon_2 - \varepsilon_3 + (\varepsilon_3 - \varepsilon_1) \cos \alpha + (\varepsilon_1 - \varepsilon_2) \cos \beta}{(\varepsilon_3 - \varepsilon_1) \sin \alpha + (\varepsilon_1 - \varepsilon_2) \sin \beta}. \quad (B9)$$

A special case of pure tension leading to the division by zero has to be considered separately.

Finally, the bending strain can be calculated using the expression:

$$\varepsilon_{B \max} = \frac{(\varepsilon_1 - \varepsilon_T)\Delta}{\sin \Delta \cos \varphi}.$$

$$\varepsilon_{B \max} = \frac{(\varepsilon_2 - \varepsilon_1) \sin \beta - (\varepsilon_3 - \varepsilon_1) \sin \alpha}{\sin \alpha - \sin \beta + \sin(\beta - \alpha)}$$

Using (B8) and the well-known relation

$$\cos \varphi = \frac{1}{\sqrt{(\tan^2 \varphi + 1)}} \text{ leads to:}$$

$$\times \sqrt{(\tan^2 \varphi + 1)} \frac{\Delta}{\sin \Delta}. \quad (\text{B10})$$